Vol 15 No 2, February 2006
1009-1963/2006/15(02)/0454-06
Chinese Physics
© 2006 Chin. Phys. Soc.
and IOP Publishing Ltd

Experimental study of noncontact ultrasonic motor with non-symmetrical electrode*

Yang Bin(杨 斌), Liu Jing-Quan(刘景全)†, Chen Di(陈 迪),
Zhou Wei-Min(周伟民), and Cai Bing-Chu(蔡炳初)

National Key Laboratory of Nano/Micro Fabrication Technology, Key Laboratory for Thin Film and Microfabrication of Ministry of Education, Institute of Micro and Nano Science and Technology, Shanghai Jiaotong University, Shanghai 200030, China

(Received 5 September 2005; revised manuscript received 20 October 2005)

We have proposed a novel noncontact ultrasonic motor based on non-symmetrical electrode driving. The configuration of this electrode and the fabrication process of rotors are presented. Its vibration characteristics are computed and analysed by using the finite element method and studied experimentally. Good agreement between them is obtained. Moreover, it is also shown that this noncontact ultrasonic motor is operated in antisymmetric radial vibration mode of B_{21} mode. The maximum revolution speed for three-blade and six-blade rotors are 5100 and 3700 r/min at an input voltage of 20V, respectively. Also, the noncontact high-speed revolution of the rotors can be realized by the parts of I, III of the electrode or II, IV of the electrode. The levitation distance between the stator and rotor is about 140μm according to the theoretical calculation and the experimental measurement.

Keywords: non-symmetrical electrode, noncontact, travelling wave, ultrasonic motor
PACC: 7760

1. Introduction

Ultrasonic motors made by using piezoelectrics need a relatively high ac electric field to excite a travelling or standing wave to drive a rotor by frictional force or acoustic radiation pressure. Compared with traditional electromagnetic motors, ultrasonic motors have many significant advantages, such as high out torque with low speed, magnetic-field-free operation, fast response, and so on. However, ultrasonic motors also have some disadvantages resulting from the frictional contact force between the stator and the rotor, including low speed and the limited working life. Therefore, it is necessary to overcome these disadvantages. Some non-contact-type motors have been proposed and investigated,[1−11] Hu *et al*[6−8] developed a motor driving fluid directly with annular symmetrical electrode and optimized operation conditions of the motor. Wang *et al*[12] proposed a piezoelectric actuator of split electrode with varying width. This will result in a bending motion of the actuator along the direction of its width. When fast movement was required, air was used because it was more difficult to saturate the sound field in air than that in others fluids.[13] For this, Yamayoshi *et al*[2,3] proposed a disc-type noncontact motor on air basis with an interdigital electrode. Furthermore, the electromechanical coupling factor can be improved in this driving way.[14] Therefore, it is easy to obtain high speed. A maximum revolution speed was 3000r/min when a voltage of $100V_{\mathrm{p-p}}$ was applied.[2] But its construction was complicated, so this kind of motor was difficult to fabricate, especially miniature motors.

In this paper, we propose a novel method for driving ultrasonic motor by using a non-symmetrical electrode. The exciting principle of travelling waves generated by this electrode is presented. The maximum rotating speed and levitation distance are measured. In the theoretical development, the three-dimensional (3D) finite element model is used to simulate the dynamic vibration characteristics of this motor. This motor has the advantages of simple structure, high revolution speed and easy miniaturization.

2. Working principle of the micromotor

Figure 1 shows the working principle of a non-

*Project supported by the National Natural Science Foundation of China (Grant No 50205017).
†E-mail: jqliu@sjtu.edu.cn

contact ultrasonic motor. The travelling wave on the stator generates a sound field in the gap between the stator and the rotor. The travelling sound field in the gap produces three unidirectional forces on the rotor.[8] The first one is in the axial direction and levitates the rotors. The second one is the viscous force in the radial direction and stabilizes the rotors. The third one induces near-boundary streaming in the circumferential direction near the surface of the rotor. The velocity gradient of the near-boundary streaming on the surface of the rotor produces a viscous force, which causes the rotor to rotate in the direction of the travelling wave along the stator.[7] But for the contact piezoelectric motor, the rotation direction of the rotor is the inverse direction of the travelling wave.

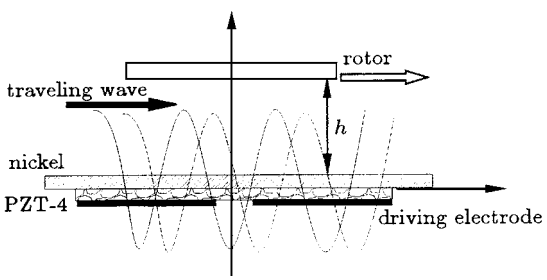


Fig.1. Principle of noncontact ultrasonic motor.

The non-symmetrical electrode construction of the parts I, II, III and IV is shown in Fig.2 (a); for comparison, Fig.2(b) also shows the symmetrical electrode construction. From Fig.2(a), the total displacement equation is given by

$$W = H\sin(\omega t - n\theta + \phi), \tag{1}$$

where

$$H = 2A\sqrt{[\cos(3n\pi/10)]^2 + [1+\sin(3n\pi/10)]^2},$$

$$\phi = \arctan\left[-\frac{\cos(3n\pi/10)}{1+\sin(3n\pi/10)}\right]. \tag{2}$$

Here $2A$ is the vibration amplitude excited by the non-symmetrical electrode, ω is the angular frequency of the stator vibration, and n is the wave number along the circumferential direction of the stator.

From Eq.(1), the vibration velocity equation of the stator is

$$v = \partial W^2/(\partial\theta\partial t) = Hn\omega\sin(\omega t - n\theta + \phi). \tag{3}$$

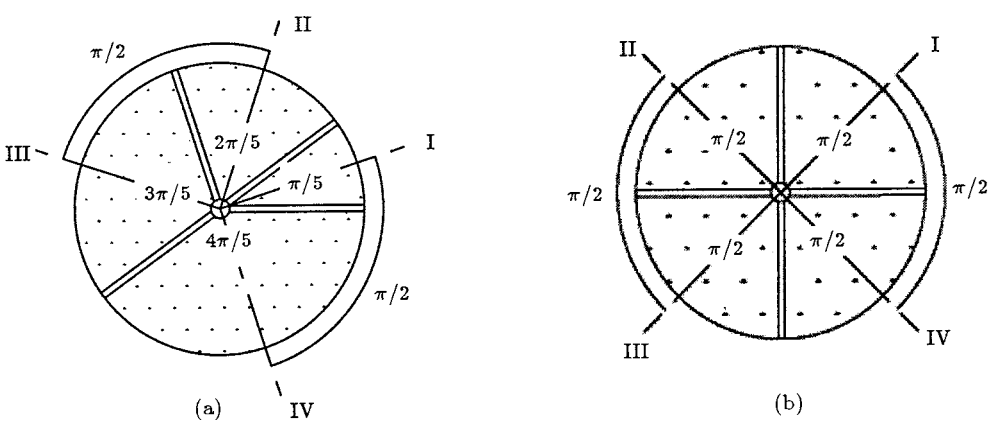


Fig.2. Construction of the electrode: (a) non-symmetrical type, (b) symmetrical type.

3. Fabrication and characteristics of a sample motor

3.1. Fabrication and driving circuit

A sample motor was fabricated according to the proposed design, and its performance was evaluated by experiment. Figure 3 is a photograph of the fabricated motor, which consists of a stator and a rotor. The stator is a composite disc made of piezoceramic and nickel discs, whose thickness and diameter are 0.17 and 10mm, 0.22 and 20mm, respectively. SU-8 photoresist is selected as the material of the rotor. The rotors are fabricated by UV-LIGA process[15] to control the rotor shape and thickness. Furthermore, the high smoothness level of rotors can be obtained. This new fabrication process of the rotor is schematically described in Fig.4. A glass wafer is prepared with a sacrificial layer (Ni / 0.1μm). A thick negative photoresist layer (SU-8/170μm) is spun with a rotating

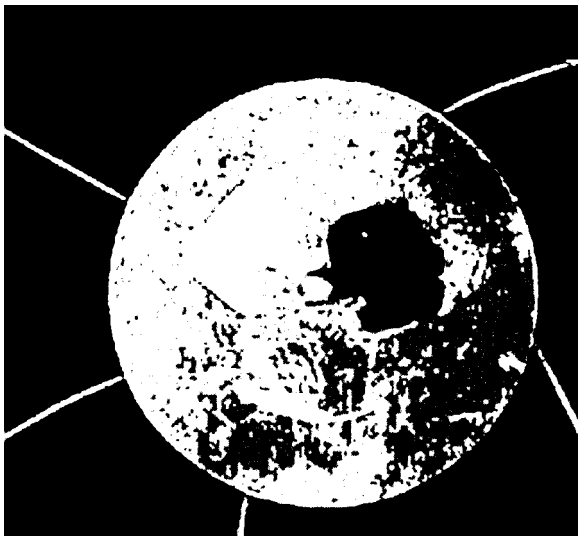


Fig.3. Photograph of a fabricated motor.

cover spinner (Karl süss RC8 Spin Coater) and prebaked in an oven at 90° for 2h (Fig.4(a)). Prebake is then followed by UV illumination (mask with the structure of rotor) and post bake in the oven to perform crosslinking. Then it is developed in PGMEA (propylenglycol-monomethylether-acetate) (Fig.4(b)). In the final step the fabricated rotors are released by a sacrificial etching of the Ni in a $FeCl_3$ (ferric chloride) solution (Fig.4(c)). Figure 5 shows the construction of three-blade and six-blade rotors. In this paper, the blade widths of three-blade and six-blade rotors are 6 and 4 mm, respectively. For both of them, the radius is 6 mm and the thickness is 0.17 mm. The corresponding weights of them are 17 and 19.4 mg, respectively, by the use of electro-optical analytical balance. Figure 6 is a schematic diagram of the driving circuit, which consists of a signal generator, a phase shifter, two amplifiers, two pulse transformers for impedance matching.

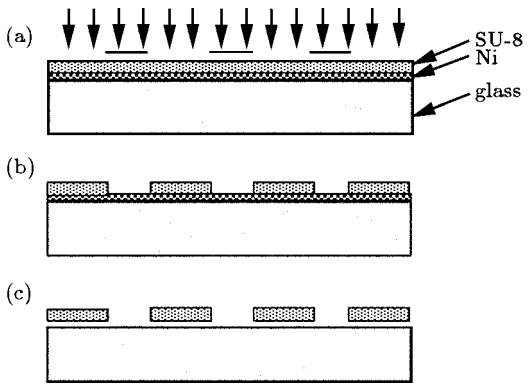


Fig.4. A flow chart of the rotors microfabrication process.

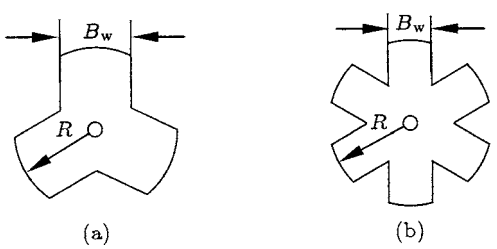


Fig.5. The construction of rotors: (a) three-blade rotor; (b) six-blade rotor.

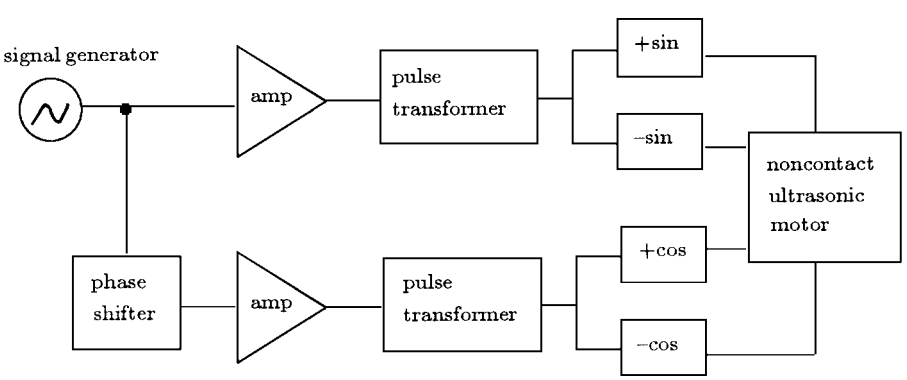


Fig.6. Block diagram of driving circuit.

3.2. Vibration analysis

The admittance spectrum measured using Agilent 4294A precision impedance analyser is given in Fig.7. It is seen from Fig.7 that the resonant frequency is about 35 kHz for parts I, II, III and IV of the electrode. To acquire steady-state response functions such as vibration modes, the dynamic modal analysis of the stator was performed using a commercially available FEM package (ANSYS 5.7). And the 3D coupling field solid elements of SOLID5 with eight modes are used to

model the piezoceramic disc. The final model consists of 5392 nodes and 4050 elements. Figure 8(a) illustrates the vibration mode of the stator, showing that the mode is B_{21} mode at 35.941kHz. In order to further verify the accuracy of the finite element model, we use the laser Doppler vibrometer (Polytec.OFV-3001S) to carry out the relative experimental measurement within the desired frequency range. Figure 8(b) shows the instantaneous vibration displacement distributions of the stator. The resonant frequency is 34kHz for B_{21} mode obtained from the experiment. Close agreement has been attained between finite element model and experimental results for both characteristics mentioned above.

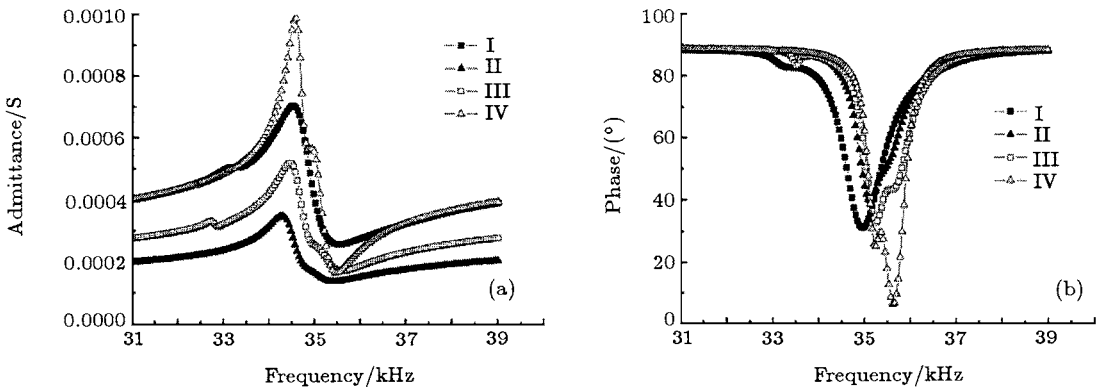


Fig.7. Admittance spectrum of the stator: (a) the relationship between admittance and frequency; (b) the relationship between phase and frequency.

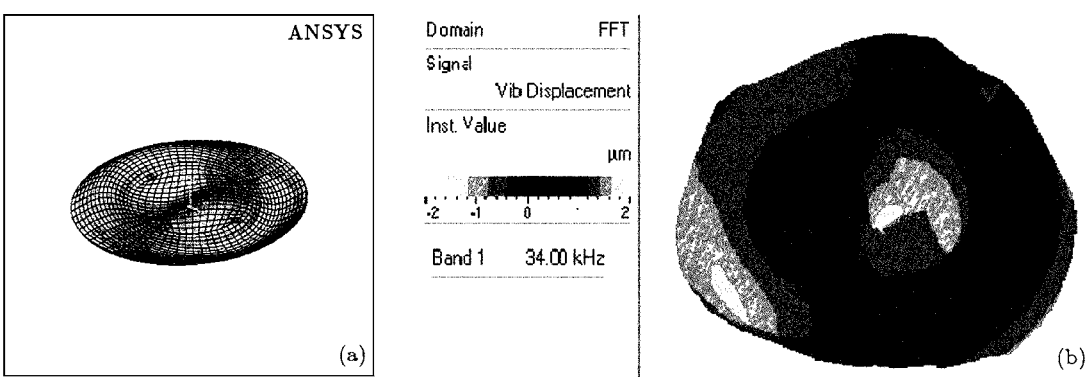


Fig.8. Ultrasonic vibration mode of the stator: (a) computed ANSYS; (b) measured experimentally.

3.3. Motor performance

Figure 9 shows the revolution speed versus driving frequency for the non-symmetrical electrode driving, with the driving voltage amplitude being 20V. The maximum revolution speeds are 5100r/min and 3700r/min at the resonant frequency for three-blade and six-blade rotors, respectively. On the other hand, it can be seen that the performance of the motor is obviously improved, as compared with the symmetrical electrode. From Fig.8(b), the vibration amplitude measured by a laser vibrometer is 2 μm at the input voltage of 20V. So the stator vibration velocity is 1.625 m/s at the resonant frequency according to Eqs.(3), and its corresponding revolution speed is 1550 r/min. The revolution speed of the rotor is far greater than it, which verifies the advantage of high revolution speed for noncontact ultrasonic motor.

Figure 10 shows how the revolution speed changes with the increase of the phase difference of two channel signals. From Fig. 10, the sinusoidal relationship between them is obtained. However, the revolution speed reaches a maximum when the phase difference approaches 70° or 250°, not 90° or 270°; this is because ϕ exists in the velocity equation of the stator from Eq.(3) and the calculated ϕ value is about 20°.

Furthermore, the rotors can revolve in clockwise or anticlockwise direction according to the phase difference of either 70°or 250° as can be seen from Fig.10.

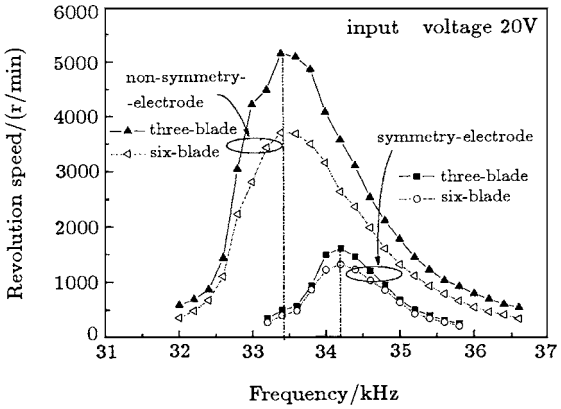


Fig.9. The relationship between the revolution speed and driving frequency.

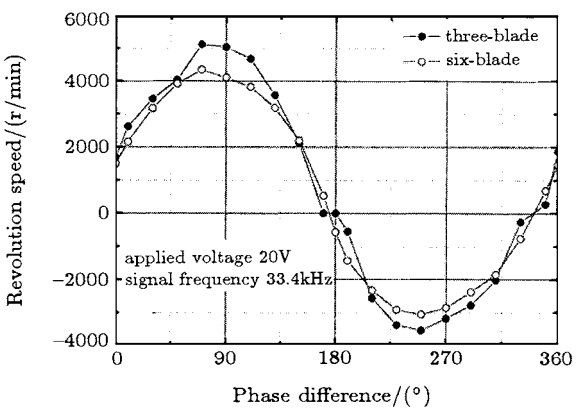


Fig.10. The relationship between the revolution speed and phase difference of two channel signals.

To simplify the driving electrical source, only single channel signal can be supplied to the noncontact ultrasonic motor revolved with high speed. Figure 11 shows the relationship between the revolution speed and signal frequency driven by the parts I, III of the electrode or the parts II, IV of the electrode. In Figs.9 and 11, the revolution speed shows a gradual increase up to the resonant frequency. From Fig.12, we can find that the revolution speed increases linearly with the driving voltage.

According to the formulation derived by Chu and Apfel,[16,9] the radiation pressure Π is expressed as

$$\Pi = \frac{1+\gamma}{4}\rho c^2 \frac{a^2}{h^2}. \qquad (4)$$

Here, γ is the specific heat ratio, ρ is the density of medium, c is the sound velocity in the medium, a is the vibration amplitude ($= v_0/\omega$).

The levitation distance computed by using Eq.(4) is 136μm for both the three-blade and six-blade rotors. In this paper, we use a CCD laser displacement transducer (KEYENCE, LK-036) to measure the levitation distance which is 140μm for both of them. The result shows that the measured value agrees with the theoretical value.

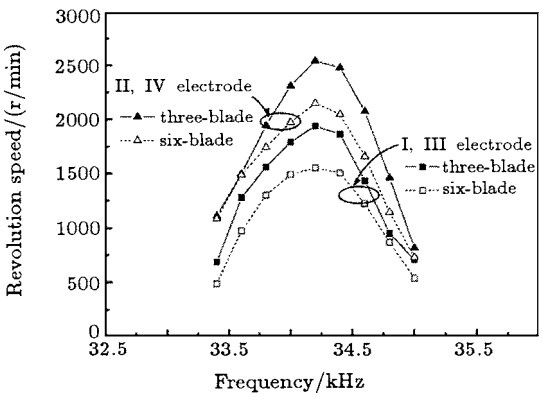


Fig.11. The relationship between the revolution speed and driving frequency of single channel signal.

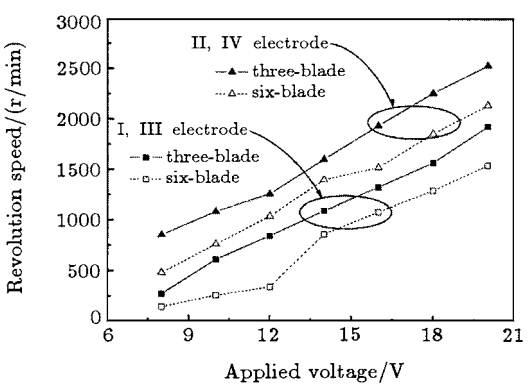


Fig.12. The relationship between the revolution speed and driving voltage of single channel signal.

4. Conclusion

We have improved the performance and simplified the driving electrode for a noncontact ultrasonic motor driven by non-symmetrical electrode. The maximum revolution speed of three-blade rotor is 5100r/min at the resonant frequency. The revolution directions of the rotors can be realized by changing the phase difference of two channel signals. The relationship between them may be explained by combined travelling wave equation. The driving mechanism using the non-symmetrical electrode is also important and there should be further studies.

References

[1] Nakamura K, Ito T, Kurosawa M and Ueha S 1990 *Jpn. J. Appl. Phys.* **29** 160

[2] Yamayoshi Y and Hirose S 1992 *Int. J. Appl. Electromagn. Mater.* **3** 179

[3] Hirose S, Yamayoshi Y and Ono H 1993 *IEEE Ultrasonics Symp.* p453

[4] Hu J H, Yamazaki T, Nakamura K and Ueha S 1995 *Jpn. J. Appl. Phys.* **34** 2702

[5] Nakamura K, Maruyama M and Ueha S 1996 *Ultrasonics* **34** 261

[6] Hu J H, Nakamura K and Ueha S 1996 *Jpn. J. Appl. Phys.* **35** 3289

[7] Yamazaki T, Hu J H, Nakamura K and Ueha S 1996 *Jpn. J. Appl. Phys.* **35** 3286

[8] Hu J H, Nakamura K and Ueha S 1997 *Ultrasonics* **35** 459

[9] Ueha S, Hashimoto Y and Koike Y 2000 *Ultrasonics* **38** 26

[10] Saito J, Friend J R, Nakamura K and Ueha S 2005 *Jpn. J. Appl. Phys.* **44** 4666

[11] Hu J H, Li G R, Chan H L W and Choy C L 2001 *IEEE Trans. Ultrason. Ferroelec. Freq. Contr.* **48** 699

[12] Wang Z H, Tiang X G, Wang S H and Yao X 1998 *Acta. Phys. Sin.* **47** 2053 (in Chinese)

[13] Hu J H 1997 *Ph. D. Tokyo institute of technology* (in Japanese) p48

[14] Ueha S and Tomikawa Y 1993 *Ultrasonic Motors— Theory and Applications* (Oxford: Clarendon) p36

[15] Chien H H, Ping C K, Rong Y C *et al* 2002 *Sensors and Actuators* A **102** 130

[16] Chu B and Apfel R E 1982 *J. Acoust. Soc. Jpn.* **72** 1673